Applied Physics Letters ARTICLE pubs.aip.org/aip/apl

Periodic lateral superlattice in bonded $SrTiO_3/SrTiO_3$ twisted perovskites

Cite as: Appl. Phys. Lett. **126**, 101902 (2025); doi: 10.1063/5.0251478
Submitted: 3 December 2024 · Accepted: 25 February 2025 ·
Published Online: 10 March 2025

M. Schmidbauer,[1,a)] J. Maltitz,[1] F. Stümpel,[1] M. Hanke,[2] C. Richter,[1] J. Schwarzkopf,[1] and J. Martin[1]

AFFILIATIONS

[1]Leibniz-Institut für Kristallzüchtung, Max-Born Str. 2, 12489 Berlin, Germany
[2]Paul-Drude-Institut für Festkörperelektronik, Hausvogteiplatz 5-7, 10117 Berlin, Germany

[a)]Author to whom correspondence should be addressed: martin.schmidbauer@ikz-berlin.de

ABSTRACT

Stacking of freestanding membranes enables the formation of interfaces beyond what can be obtained with classical heteroepitaxy. In particular, twisted interfaces provide unique physical properties not existent in the corresponding individual layers. An ideal twist grain boundary yields an in-plane screw-dislocation network, assuming sufficiently strong interactions across the interface, for example, via covalent or ionic bonding. Hereby, the distance between dislocation lines, that is the length scale of the Moiré pattern, is set by the twist angle between the adjacent crystalline surfaces and the lattice mismatch in case that different materials are placed together. The associated strain gradients of the periodic pattern are especially appealing for oxide-based perovskites due to the intricate connection between surface polarization and subtle structural deformations such as the oxygen octahedra tilt. Recently, freestanding oxide perovskites became available via the sacrificial layer approach, opening a pathway toward oxide-based Moiré materials. Here, we demonstrate efficient bonding of a freestanding $SrTiO_3$ layer to a $SrTiO_3$ single-crystal by initially conducting a wafer-bonding process at high temperature and only subsequently dissolving the sacrificial layer. We investigate the twisted $SrTiO_3/SrTiO_3$ interface with x-ray diffraction in grazing incidence geometry and observe clear signatures of a highly periodic lateral superlattice consistent with the formation of a screw-dislocation network. Our work demonstrates a robust route for the fabrication of twisted perovskites and their development into a functional material platform with designed strain gradients at the nanoscale.

The transfer of freestanding crystalline films is gaining importance as an alternative approach to tune material properties and device performance. Layer transfer enables unique material combinations and interfaces, which could not be grown by classical heteroepitaxy. In particular, it allows control of the relative in-plane orientation of the layers, thereby forming twisted interfaces and Moiré materials [Fig. 1(a)]. Moiré materials constitute an innovative class of material interfaces in which (opto-)electronic properties are tuned by the relative twist angle of the adjacent crystalline surfaces.[1] For two-dimensional (2D) van der Waals materials, Moiré materials are exploited for band structure engineering revealing correlated electronic phases.[2,3] Furthermore, the periodic Moiré potential gives rise to minibands and band gaps resulting in additional quantum Hall states.[4] The Moiré potential also affects optoelectronic properties such as the exciton binding energy and diffusion.[5–7] Likewise, the optoelectronic properties of Moiré structures are also investigated in the emerging field of 2D-hybrid perovskites.[8] In both material systems, the relatively weak interlayer interaction renders strain and structural relaxation a minor role, relevant mostly in the limit of small twist angles.[9,10] This is different when considering oxide-based perovskites such as $SrTiO_3$ with strong bonding across layers. In this case, structural reconstructions and their associated strain fields are crucial for all twist angles.

Strain-engineering of functional materials as such is a well-established technology for tuning material properties and optimizing device performances. Often, heteroepitaxy is utilized to establish lattice strain in thin films by introducing a lattice mismatch between film and substrate. The most common concept of plastic relaxation of epitaxial mismatch strain at interfaces is the formation of misfit dislocations. While these always involve an edge component, pure screw-dislocation networks that are topologically required at twist boundaries[11] are much less explored. Such pure twist boundaries are rare in epitaxially grown films, but can be artificially realized for virtually any combination of perovskite via hot pressing of single-crystals,[12] sintering,[13] wafer bonding,[14] or by thin film layer transfer.[15,16] As benefit, the transfer of thin layers provides near-surface access for structural investigations. Strong interlayer interactions favor to maximize the

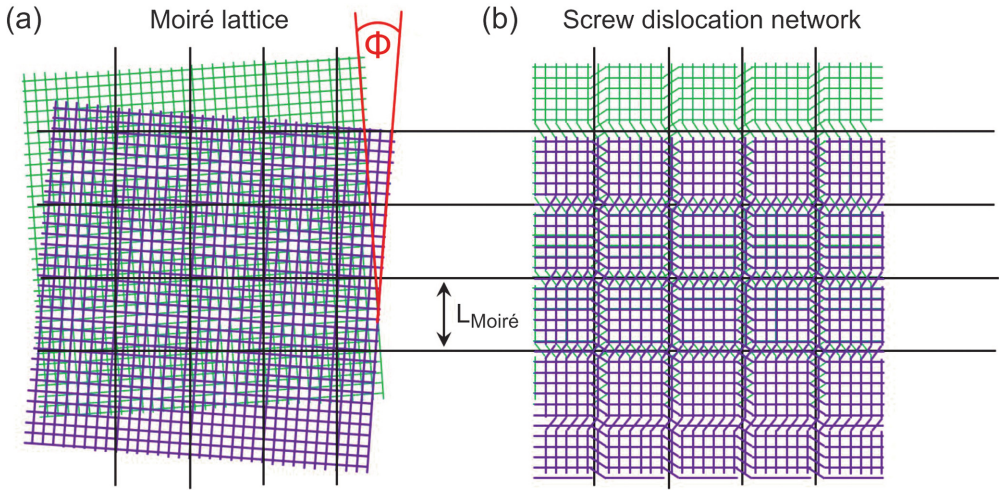

FIG. 1. (a) Formation of a periodic Moiré pattern by the overlay of two twisted quadratic lattices with identical lattice parameters. (b) Scheme of a periodic screw-dislocation network located at the interface showing a squared supercell with dimension of $L_{Moiré}$.

number of interatomic bonds. Hence, within each Moiré plaquette, a coherent interface between the two surfaces is formed [Fig. 1(b)]. In between these coherent areas, the structural strain is relaxed via screw dislocations. The distance between dislocations L is determined by the length scale of the Moiré pattern, which itself is controlled by the applied twist angle ϕ.

Strain can stabilize exotic crystallographic phases, thus inducing completely redesigned physical properties in a material. This approach is, for example, used to explore innovative ferroelectric materials and their applications in thin films.[17–19] Specifically, oxide perovskites are known for their rich phase diagrams that allow for the coexistence of multiple (ferroic) functional properties, which are strongly susceptible to lattice strain.[20] The superlattice resulting from the periodic strain modulation may lead to a periodic modulation of the physical properties, thus enabling alternative ways of nano-engineering. Twisted perovskites could be exploited for ferroelectric domain control, formation of mini-bands in 2D-electron gases at polar/non-polar interfaces, or could act as a template for the subsequent growth of regular arrays of self-assembled 0D- or 1D-nanostructures. Not at last, the local strain pattern imposed by the dislocation network causes a flexoelectric response in interplay with piezo-, ferroelectricity, and electrostriction.

As stated above, for the practical realization of twisted perovskites, freestanding films are needed. Recently, freestanding oxide perovskites became available following the sacrificial layer approach[21] and remote epitaxy.[22] Freestanding layers are interesting in their own right displaying phenomena distinct from bulk behavior.[23,24] Yet, stacking and twisting oxide layers is investigated with the goal to create extraordinary interfaces. While some authors claim that mere transfer is sufficient to create strong interlayer interaction and structural reconstruction,[16,17] others utilize an additional annealing step.[15,25]

Our approach involves an epitaxial $SrTiO_3/(Ca,Sr)_3Al_2O_6$ layer system grown on $SrTiO_3$ substrate, which was subsequently bonded to a $SrTiO_3$ substrate via an annealing step. Thereby the $(Ca,Sr)_3Al_2O_6$ layer is water-soluble and serves as a sacrificial layer (a schematic of the procedure is shown in Fig. S1). For this purpose, both the $SrTiO_3$ epi-substrate and the $SrTiO_3$ bonding substrate have been prepared according to Ref. 26 to provide a TiO_2-surface termination. The surface topography recorded by atomic force microscopy (AFM) in peak force tapping mode (Bruker Icon dimension) displays an atomically smooth step-and-terrace surface structure with a step width of approximately 200 nm, which can be expected for an off-cut angle of 0.1° [Fig. S2(a)]. We use pulsed laser deposition (PLD) for epitaxial growth of sacrificial and functional layer. The PLD-target of $SrTiO_3$ was provided from Pi-Kem Ltd, UK, while the $(Ca,Sr)_3Al_2O_6$ target has been prepared in-house using a solid-state sintering process. The Ca-content was determined by x-ray powder diffraction to be $Ca_{1.2}Sr_{1.8}Al_2O_6$, which provides the same pseudocubic lattice parameter than $SrTiO_3$. Our PLD setup is equipped with a KrF laser ($\lambda = 248$ nm) and the target-substrate distance was fixed to 50 mm. For the epitaxy of both $(Ca,Sr)_3Al_2O_6$ and $SrTiO_3$ films, the growth parameters were fixed to a laser fluence of 1.4 J cm^{-2}, a laser pulse frequency of 2 Hz and a substrate temperature of 750 °C with a heating rate of 10 K min^{-1}, while the oxygen partial pressure was kept to 0.1 mbar during the whole process.

We have performed high-resolution x-ray diffraction (HR-XRD) on a 9 kW SmartLab system (Rigaku) using Cu $K\alpha_1$ radiation ($\lambda = 1.54059$ Å). For the as-grown heterostructure, a 2θ-ω-scan in the vicinity of the 002 $SrTiO_3$ Bragg reflection is shown in Fig. 2(a). The sharp substrate peak at $2\theta = 46.47°$ is surrounded by pronounced Laue oscillations originating from the $SrTiO_3$ and $Ca_{1.2}Sr_{1.8}Al_2O_6$ films and indicating smooth interfaces. As the vertical lattice parameters are very similar, however, no separate film peaks can be identified but can only be recognized by a slight asymmetric broadening of the substrate peak. Simulations [red dotted curve in Fig. 2(a)] based on dynamical diffraction theory were used to determine corresponding film thicknesses of 10 nm for $SrTiO_3$ and 12 nm for $Ca_{1.2}Sr_{1.8}Al_2O_6$.

For bonding the $SrTiO_3$-layer onto the $SrTiO_3$ target substrate, we utilize a specially designed clamping mechanism (Fig. S3). The assembly of as-grown heterostructure and the target substrate is manual and allows only a rough adjustment of the twist angle. For small twist angles, we align layer and target substrate such that the direction of the surface miscut, which is typically [100], is adjusted. We estimate

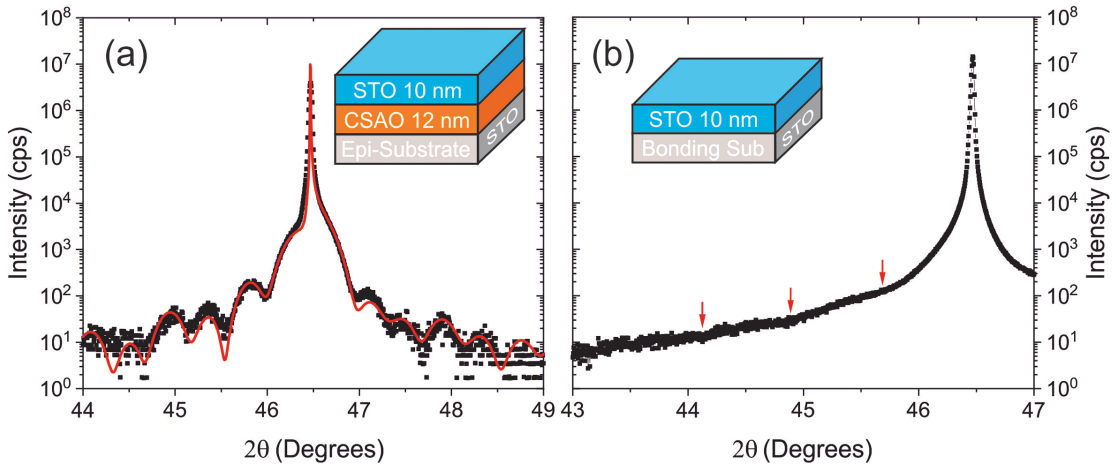

FIG. 2. (a) 2Θ-ω-scan of as-grown sample measured in the vicinity of the out-of-plane 002 Bragg reflection (black squares) along with simulation (red line). The pronounced Laue oscillations indicate a thickness of 10 nm $SrTiO_3$ (STO) and 12 nm $(Ca,Sr)_3Al_2O_6$ (CSAO). (b) The corresponding 2Θ-ω-scan of the $SrTiO_3$ film bonded onto the $SrTiO_3$ substrate. The minima positions of the very weak Laue oscillations (marked by red arrows) indicate a film thickness of $t = (10 \pm 1)$ nm.

that the clamp produces a force in the range of 10–20 N which corresponds to a pressure of about 1–2 MPa. In order to minimize the risk of accidental cracking of the brittle $SrTiO_3$ substrates, we employ a thin layer of alumina paste (typical grain size of 0.5 μm, mixed with water) serving as a soft cushion for the $SrTiO_3$ substrate. The clamping arrangement is placed inside an ambient annealing oven. Similar to the PLD-target sintering process, we ramp up to 1000 °C with a rate of 200 K/h and keep the target temperature for 1 h before cooling down with 200 K/h. The bonded structure is then released and placed in a tempered bath of DI-water at 60 °C for approximately 12 h to dissolve the sacrificial layer. Figure S4 shows an optical image of the accomplished sample proving a transferred film on the macroscopic length scale. In the corresponding surface morphology [Figs. S2(b) and S2(c)] a step-and-terrace structure can still be resolved although it is dominated by adsorbents and defects.

For structural analysis of the bonded film, a 2θ-ω HR-XRD scan in the vicinity of the out-of-plane 002 Bragg reflection of $SrTiO_3$ is carried out [Fig. 2(b)]. In addition to the sharp substrate reflection at $2\theta = 46.47°$, weak Laue oscillations can be identified, proving a smooth surface and interface and revealing a film thickness of about $t = (10 \pm 1)$ nm. From the angular positions of the intensity minima, it can be concluded that—within our experimental accuracy—the film and substrate reflections appear at the same 2θ-value, indicating identical vertical lattice parameters. Corresponding out-of-plane reciprocal space maps (see Fig. S5) confirm this observation. The Laue oscillations are, therefore, not caused by a globally different vertical lattice parameter of the film as compared to the substrate, but they are presumably created by a tiny vertical lattice phase shift at the interface. This is supported by the corresponding simulations of the experimental curve (see Fig. S6). The mechanism responsible for this phenomenon has yet to be elucidated. It could, for example, be attributed to a small "buckling-effect," caused by locally incomplete bonding at the interface.

In order to obtain additional information about in-plane lattice strains, twist angle, and the average morphology of the Moiré pattern, we performed grazing incidence in-plane x-ray diffraction (GIXD). The experiment was carried out at BM25B beamline at the European Synchrotron Radiation Facility (ESRF) using an energy of 18 keV ($\lambda = 0.6888$ Å). The glancing angle of incidence was chosen slightly above the critical angle of total external reflection of $SrTiO_3$ ($\alpha_c = 0.14°$[27]) to ensure maximum sensitivity to the thin film and regions close to the interface between the thin film and the substrate. Incident slits were chosen such that the footprint of the x-ray beam on the sample was about 5×0.2 mm^2. The diffracted signal was recorded by an area detector (Eiger, Dectris) with a pixel size of 75×75 μm^2. The very well in-plane collimation of the primary beam enables a very accurate determination of the in-plane twist angle of better than 0.01°, while the experimental resolution in 2θ-direction—defined by a collimating slit system between sample and detector—is approximately given by $\Delta(2\theta) \approx 0.05°$. Therefore, all features in the experimental 2D intensity distributions appear line-like rather than point-like. For the two measured Bragg reflections, 200 and 110, the respective experimental resolution element is sketched as a green line in Fig. 3. Additional measurements were conducted at the PHARAO beamline[28] at BESSY II, albeit with diminished angular resolution.

Figures 3(a) and 3(b) display 2D diffraction patterns in the vicinity of the 200 and 110 in-plane Bragg reflections, respectively. For both Bragg reflections, two strong peaks can be identified, which are caused by the film (F) and the substrate (S). Please note that the (200) and (110) net-planes differ by a 45° in-plane rotation. Independent of the chosen Bragg reflection, the separation of film and substrate peaks always occurs in angular direction, i.e., perpendicular to the scattering vector, while their positions in radial direction, i.e., along the scattering vector, are identical. This proves that film and substrate exhibit identical in-plane lattice parameters and are solely different in the in-plane orientation ("twist"). From the observed peak, splitting a twist angle of $\varphi = 0.80°$ can be evaluated.

In addition to the two main peaks, weak but sharp satellite reflections are identified. More precisely, the satellite reflections form a two-dimensional square lattice aligned along the Q_{100} and Q_{010} in-plane directions. The square lattice is most evident in the case of the 200 Bragg reflection [Fig. 3(a)], whereas it is considerably less pronounced

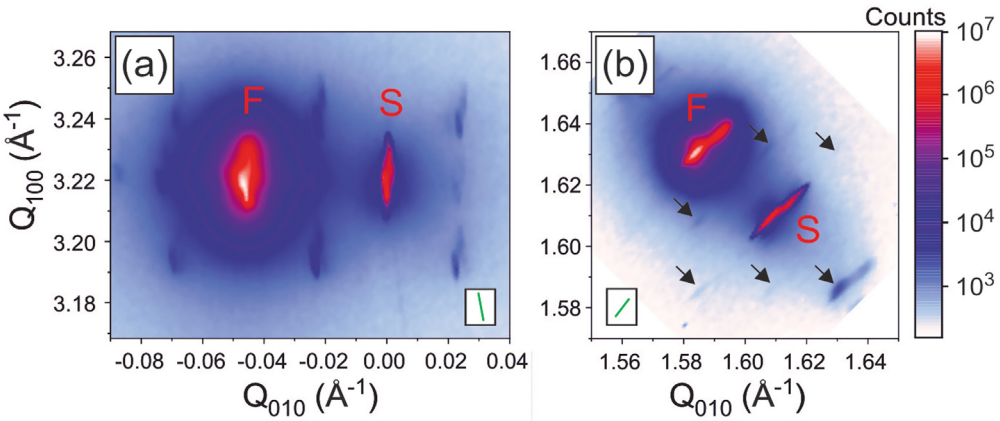

FIG. 3. Grazing incidence x-ray diffraction (GIXD) patterns in the vicinity of the (a) 200 and (b) 110 $SrTiO_3$ in-plane Bragg reflections. The substrate and film peaks are marked as "S" and "F," respectively. The green lines within the white boxes indicate the corresponding experimental resolution elements. The peculiar peak shapes are the result of experimental artifacts.

in the vicinity of the 110 Bragg reflection, where it is highlighted by black arrows [Fig. 3(b)]. It is of particular importance that both the orientation and the dimensions of the square lattices are identical for both Bragg reflections, i.e., independent of the **Q**-vector. This proves that they are generated by a two-dimensional superstructure in real space.

For the 200 Bragg reflection selected, 1D sections through some satellite reflections along radial and angular directions are displayed in the supplementary material [Figs. S7(a) and S7(b), respectively]. From a quantitative analysis a peak spacing of $\Delta Q_{100} = \Delta Q_{010} = 2.34 \times 10^{-2}$ Å^{-1} is derived. With the relation between superlattice period L_{Super} and peak spacing ΔQ in reciprocal space,

$$L_{Super} = 2\pi/\Delta Q, \quad (1)$$

a real space periodicity of $L_{Super} = (27 \pm 1)$ nm can be calculated. For comparison, we have calculated the length scale $L_{Moiré}$ of the characteristic Moiré pattern (i.e., the dimension of the "supercell") of two superimposed twisted quadratic lattices as a function of the twist angle ϕ according to[29,30]

$$L_{Moiré} = (a/2)/\sin(\phi/2). \quad (2)$$

If using the $SrTiO_3$ lattice parameter of $a = 3.9053$ Å[31] and the experimentally derived twist angle of $\phi = (0.80 \pm 0.01)°$, we obtain $L_{Moiré} = (28 \pm 1)$ nm, in excellent agreement with the value derived from Eq. (1) and much smaller than the terrace width of 200 nm.

In order to interpret our experimental results in Fig. 3, a periodic structure with a well-defined in-plane supercell must have formed at the interface between substrate and layer. It is particularly important to emphasize that the relative (symmetrical) position of the square satellite pattern with respect to the substrate (S) and film (F) reflections proves that the superstructure is commensurate with the film and substrate lattices. The prerequisite for such a superlattice is the presence of chemical bonds at the interface, which necessitates structural relaxation by the formation of screw-dislocations. Due to the macroscopically homogenous film and substrate, we expect equidistant screw-dislocations and thus the generation of a periodic network at the interface. However, the associated distortion field of this buried network is not only located directly at the film–substrate interface but gradually decays with 1/z perpendicular to the film/substrate interface,[32] i.e., toward the sample surface and the substrate. In order to obtain a detailed view of the complex strain scenario, we have used the extended finite element method (XFEM)[33] to numerically simulate the full 3D strain tensor ε_{ij}. Here, we assume an ideal twist boundary with a periodic orthogonal network of pure screw-dislocations buried 10 nm below the sample surface with in-plane Burgers vectors and corresponding (in-plane) dislocation lines along [100] and [010]. Therefore, the only strain components to be expected are shear strains, while all normal components, ε_{11}, ε_{22}, and ε_{33}, are essentially zero throughout. In Fig. 4, the in-plane shear component ε_{12} is displayed, which is strongest directly at the interface and effectively penetrates into the underlying substrate and twisted film.

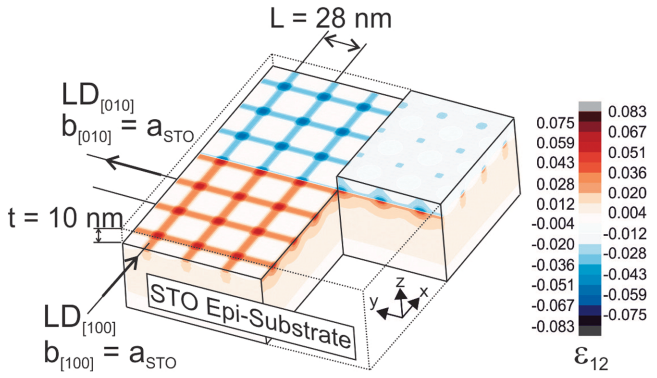

FIG. 4. Simulation of the in-plane strain component ε_{12} derived from the extended finite element method. We assume an orthogonal periodic array of pure screw-dislocations buried 10 nm below the sample surface and aligned along the ⟨100⟩ line directions. Partially translucent areas facilitate insight into the strain field at specific locations. The left-hand side of the figure depicts the areas situated directly below and above the interface, while the right-hand side illustrates the situation at the surface. Furthermore, both vertical planes situated at the dislocation core (y–z plane) and between two adjacent dislocation lines (x–z plane) provide a detailed insight into the vertical decay of ε_{12}.

It is important to stress that the origin of the observed rotational Moiré pattern is exclusively an in-plane twist between the film and substrate with identical in-plane lattice parameters. This is clearly evidenced by the observed x-ray intensity patterns (Fig. 3), as the length of the in-plane scattering vector is identical for film and substrate peaks, and the peak splitting occurs perpendicular to the scattering vector. In general, translational Moiré patterns can also arise when two lattices with slightly different lattice parameters are oriented parallel to each other, for example, for the interface between a relaxed $SrTiO_3$ film and an underlying $(LaAlO_3)_{0.3}(Sr_2TaAlO_6)_{0.7}$ substrate.[34] Even mixed Moiré patterns can appear when periodic lattices with slightly different lattice parameters are rotated to each other.[35] For these translational Moiré patterns, the corresponding x-ray diffraction patterns differ significantly from those observed in this work, so that we can discard these patterns for our sample.

Finally, within our experimental accuracy, we did not observe any remarkable out-of-plane tilt angle of the bonded thin film with respect to the substrate. From the out-of-plane reciprocal space maps shown in Fig. S4, we can estimate an upper limit of the tilt angle of 0.05°. This shows, that the $SrTiO_3$ film is homogeneously bonded to the substrate on a macroscopic scale. As a result, the dislocations at the interface are expected to be of pure screw type with in-plane Burgers vector, while edge type or mixed dislocations should occur very rarely.[14]

In summary, the results presented herein provide compelling evidence for the formation of a periodic screw-dislocation network at the interface between the twisted $SrTiO_3$ thin film and the $SrTiO_3$ substrate. In particular, the emergence of high-order superlattice peaks and corresponding sharp line widths indicate the presence of a well-ordered interface, which is a consequence of a homogeneous transfer and subsequent bonding of the film onto the substrate. To gain further insight into the inhomogeneous strain field associated with the screw-dislocation network, more sophisticated x-ray studies are required. These involve, in particular, the measurement of weak diffuse scattering in the proximity of the superlattice Bragg reflections. In addition, an in-depth characterization of the interfacial atomic structure using advanced electron microscopy techniques[17] is envisioned for the future.

See the supplementary material for additional experimental details regarding the fabrication, characterization, and extended HR-XRD measurements.

We are grateful to ESRF (Grenoble) and BESSY II (Helmholtz-Zentrum Berlin) for granting beam time (Experiment Nos. HC-5796 and 222-11326-CR, respectively). We also acknowledge technical support with the synchrotron measurements from Juan Rubio Zuazo and Ana Garcia Prieto (BM25, ESRF) and from Steffen Behnke (Paul-Drude-Institut, Berlin). We are grateful to Uwe Jendritzki for the design of the clamping mechanism, and to Christopher Kleinig for support in wafer bonding and annealing. We thank DFG for the grant "nano-twist" Nos. MA 9075/1-1, SCHW 1500/9-1, and the European Regional Development Fund ERDF (Project No. 1.8/15).

AUTHOR DECLARATIONS

Conflict of Interest

The authors have no conflicts to disclose.

Author Contributions

M. Schmidbauer: Formal analysis (lead); Investigation (equal); Writing – original draft (equal). **J. Maltitz:** Investigation (equal); Methodology (lead); Writing – review & editing (supporting). **F. Stümpel:** Investigation (supporting); Methodology (supporting). **M. Hanke:** Investigation (equal); Writing – review & editing (supporting). **C. Richter:** Investigation (supporting); Writing – review & editing (supporting). **J. Schwarzkopf:** Conceptualization (equal); Project administration (equal); Writing – review & editing (supporting). **J. Martin:** Conceptualization (equal); Project administration (equal); Writing – original draft (equal).

DATA AVAILABILITY

The data that support the findings of this study are available from the corresponding author upon reasonable request.

REFERENCES

[1]J. C. W. Song and N. M. Gabor, Nat. Nanotechnol. **13**, 986–993 (2018).
[2]Y. Cao, V. Fatemi, A. Demir, S. Fang, S. L. Tomarken, J. Y. Luo, J. D. Sanchez-Yamagishi, K. Watanabe, T. Taniguchi, E. Kaxiras, R. C. Ashoori, and P. Jarillo-Herrero, Nature **556**, 80–84 (2018).
[3]Y. Cao, V. Fatemi, S. Fang, K. Watanabe, T. Taniguchi, E. Kaxiras, and P. Jarillo-Herrero, Nature **556**, 43–50 (2018).
[4]Y. Cao, J. Y. Luo, V. Fatemi, S. Fang, J. D. Sanchez-Yamagishi, K. Watanabe, T. Taniguchi, E. Kaxiras, and P. Jarillo-Herrero, Phys. Rev. Lett. **117**, 116804 (2016).
[5]K. Tran, G. Moody, F. Wu, X. Lu, J. Choi, K. Kim, A. Rai, D. A. Sanchez, J. Quan, A. Singh, J. Embley, A. Zepeda, M. Campbell, T. Autry, T. Taniguchi, K. Watanabe, N. Lu, S. K. Banerjee, K. L. Silverman, S. Kim, E. Tutuc, L. Yang, A. H. MacDonald, and X. Li, Nature **567**, 71–75 (2019).
[6]C. Jin, E. C. Regan, A. Yan, M. I. B. Utama, D. Wang, S. Zhao, Y. Qin, S. Yang, Z. Zheng, S. Shi, K. Watanabe, T. Taniguchi, S. Tongay, A. Zettl, and F. Wang, Nature **567**, 76–80 (2019).
[7]Z. Li, X. Lu, D. F. C. Leon, Z. Lyu, H. Xie, J. Hou, Y. Lu, A. Kaczmarek, Z. Lyu, T. Taniguchi, K. Watanabe, L. Zhao, L. Yang, and P. B. Deotare, ACS Nano **15**, 1539–1547 (2021).
[8]S. Zhang, L. Jin, Y. Lu, L. Zhang, J. Yang, Q. Zhao, D. Sun, J. J. P. Thompson, B. Yuan, K. Ma, Akriti, J. Y. Park, Y. H. Lee, Z. Wei, B. P. Finkenauer, D. D. Blach, S. Kumar, H. Peng, A. Mannodi-Kanakkithodi, Y. Yu, E. Malic, G. Lu, L. Dou, and L. Huang, Nat. Mater. **23**, 1222–1229 (2024).
[9]Y. Bai, L. Zhou, J. Wang, W. Wu, L. J. McGilly, D. Halbertal, C. F. B. Lo, F. Liu, J. Ardelean, P. Rivera, N. R. Finney, X.-C. Yang, D. N. Basov, W. Yao, X. Xu, J. Hone, A. N. Pasupathy, and X.-Y. Zhu, Nat. Mater. **19**, 1068–1073 (2020).
[10]R. Engelke, H. Yoo, S. Carr, K. Xu, P. Cazeaux, R. Allen, A. M. Valdivia, M. Luskin, E. Kaxiras, M. Kim, J. H. Han, and P. Kim, Phys. Rev. B **107**, 125413 (2023).
[11]W. Bollmann, *Crystal Defects and Crystalline Interfaces* (Springer, Berlin, Heidelberg, Germany, 1970).
[12]H. F. Fischmeister, G. Elssner, B. Gibbesch, K. -H. Kadow, F. Kawa, D. Korn, W. Mader, and M. Turwitt, Rev. Sci. Instrum. **64**, 234–242 (1993).
[13]D. Dimos, P. Chaudhari, and J. Mannhart, Phys. Rev. B **41**, 4038 (1990).
[14]L. A. Hughes and K. van Benthem, J. Am. Ceram. Soc. **102**, 578 (2019).
[15]Y. Li, C. Xiang, F. M. Chiabrera, S. Yun, H. Zhang, D. J. Kelly, R. T. Dahm, C. K. R. Kirchert, T. E. Le Cozannet, F. Trier, D. V. Christensen, T. J. Booth, S. B. Simonsen, S. Kadkhodazadeh, T. S. Jespersen, and N. Pryds, Adv. Mater. **34**, 2203187 (2022).
[16]G. Sánchez-Santolino, V. Rouco, S. Puebla, H. Aramberri, V. Zamora, M. Cabero, F. A. Cuellar, C. Munuera, F. Mompean, M. Garcia-Hernandez, A. Castellanos-Gomez, J. Íñiguez, C. Leon, and J. Santamaria, Nature **626**, 529–534 (2024).
[17]H. Sha, Y. Zhang, Y. Ma, W. Li, W. Yang, J. Cui, Q. Li, H. Huang, and R. Yu, Nat. Commun. **15**, 10915 (2024).
[18]D. G. Schlom, L.-Q. Chen, C.-B. Eom, K. M. Rabe, S. K. Streiffer, and J.-M. Triscone, Annu. Rev. Mater. Res. **37**, 589–626 (2007).

[19]A. M. Glass and E. M. Lines, *Principles and Applications of Ferroelectrics and Related Materials*, Oxford Classic Texts in the Physical Sciences (Clarendon Press, Oxford, 2009).
[20]J. M. Rondinelli and N. A. Spaldin, Adv. Mater. **23**, 3363 (2011).
[21]D. Lu, D. J. Baek, S. S. Hong, L. F. Kourkoutis, Y. Hikita, and H. Y. Hwang, Nat. Mater. **15**, 1255 (2016).
[22]H. Yoon, T. K. Truttmann, F. Liu, B. E. Matthews, S. Choo, Q. Su, V. Saraswat, S. Manzo, M. S. Arnold, M. E. Bowden, J. K. Kawasaki, S. J. Koester, S. R. Spurgeon, S. A. Chambers, and B. Jalan, Sci. Adv. **8**, eadd5328 (2022).
[23]S. S. Hong, J. H. Yu, D. Lu, A. F. Marshall, Y. Hikita, Y. Cui, and H. Y. Hwang, Sci. Adv. **3**, eaao5173 (2017).
[24]D. Pesquera, A. Fernández, E. Khestanova, and L. W. Martin, J. Phys.: Condens. Matter **34**, 383001 (2022).
[25]H. Wang, V. Harbola, Y. -J. Wu, P. A. van Aken, and J. Mannhart, Adv. Mater. **36**, 2405065 (2024).
[26]M. Kawasaki, K. Takahashi, T. Maeda, R. Tsuchiya, M. Shinohara, O. Ishiyama, T. Yonezawa, M. Yoshimoto, and H. Koinuma, Science **266**, 1540–1542 (1994).
[27]See https://x-server.gmca.aps.anl.gov/x0h.html for "calculating the critical angle of total external reflection."
[28]B. Jenichen, W. Braun, V. M. Kaganer, A. G. Shtukenberg, L. Däweritz, C.-G. Schulz, K. H. Ploog, and A. Erko, Rev. Sci. Instrum. **74**, 1267 (2003).
[29]J. Kim, K. Kim, and Z. Lee, Sci. Rep **5**, 12508 (2015).
[30]S. Carr, S. Fang, and E. Kaxiras, Nat. Rev. Mater. **5**, 748–763 (2020).
[31]M. Schmidbauer, A. Kwasniewski, and J. Schwarzkopf, Acta Cryst. B **68**, 8–14 (2012).
[32]P. M. Anderson, J. P. Hirth, and J. Lothe, *Theory of Dislocations*, 3rd ed. (Cambridge University Press, Cambridge, 2017).
[33]E. Wintersberger, N. Hrauda, D. Kriegner, M. Keplinger, G. Springholz, J. Stangl, G. Bauer, J. Oswald, T. Belytschko, C. Deiter, F. Bertram, and O. H. Seeck, Appl. Phys. Lett **96**, 131905 (2010).
[34]M. Burian, B. F. Pedrini, N. O. Hernandez, H. Ueda, C. A. F. Vaz, M. Caputo, M. Radovic, and U. Staub, Phys. Rev. Res. **3**, 013225 (2021).
[35]M. Yankowitz, J. Xue, D. Cormode, J. D. Sanchez-Yamagishi, K. Watanabe, T. Taniguchi, P. Jarillo-Herrero, P. Jacquod, and B. J. LeRoy, Nat. Phys. **8**, 382–386 (2012).